Plastic flow under compression and shear in rotational diamond anvil cell: Finite-element study

Valery I. Levitas[a] and Oleg M. Zarechnyy
Department of Mechanical Engineering, Texas Tech University, Lubbock, Texas 79409, USA

(Received 15 August 2007; accepted 15 September 2007; published online 5 October 2007)

Plastic flow and the evolution of distribution of the components of stress tensor in a sample under compression and shear in rotational diamond anvil cell are studied using the finite-element method (FEM). Pressure self-multiplication effect is revealed during rotation of an anvil after compression below critical force. Significant heterogeneity of accumulated plastic strain (especially near contact surface with diamond) is found. The obtained results are important for determination and interpretation of kinetics of strain-induced phase transformations (PTs) and chemical reactions. © *2007 American Institute of Physics*. [DOI: 10.1063/1.2794431]

Rotational diamond anvil cell (RDAC) (see the inset of Fig. 1) is used to study unique materials behavior under high pressure and large plastic shear deformations.[1–3] It is known that the addition of plastic shear under fixed load, due to the rotation of an anvil, leads to the following results: (1) a significant reduction (by a factor of 3–5) in PT pressure and pressure hysteresis; (2) an appearance of new phases, which were not obtained without additional shear; (3) replacement of a reversible PT by an irreversible PT, and (4) strain-controlled kinetics (see[1–5]). To understand these phenomena and find methods to control them, it is necessary to understand the stress state and plastic flow of the deformed material. Knowledge on the stress state combined with x-ray measurements of distances between atomic planes may lead to more accurate determination of the elastic properties of materials. Also, despite the significant efforts to determine all components of stress tensor experimentally, reliable data are currently obtained for the mean pressure only. FEM offers distribution of all components of stress tensor. While plastic flow under compression has been studied in[6,7] using FEM, it has not been studied under compression and shear. The only existing analytical solution to this problem[4,5] contains a number of simplifying assumptions. In this paper, we present the results of a FEM study of a sample under compression and shear in RDAC.

A linear elastic, perfectly plastic model with von Mises plasticity condition $\sigma_i=\sigma_y$ is used,[8] where σ_i and σ_y are the stress intensity and the yield strength, respectively. Elastic strains are assumed to be small (<0.1), so pressure is limited to $0.1K$, where K is the bulk modulus. Then, we can neglect the deformations of the anvils. We used $K=175$ GPa, $\mu=0.2525$, and $\sigma_y=1.6$ GPa, which are typical to strengthened steel. All stresses can be normalized by σ_y. For a thin disk under pressure exceeding $2\sigma_y$, asperities of the diamond penetrate into a deformed sample. This leads either to complete cohesion or when the shear friction stress along contact anvil-sample surface, $\tau=\sqrt{\tau_{rz}^2+\tau_{\varphi r}^2}$, reaches the yield stress in shear $\tau_y=\sigma_y/\sqrt{3}$, sliding within a thin layer of a sample material. Here, τ_{rz} and $\tau_{\varphi r}$ are the shear contact stresses in the radial and twisting directions. These conditions can be modeled by complete cohesion between sample and anvils along the line OAD (Fig. 1). In the part of the contact region OA where τ approaches τ_y, large plastic shear is localized in the first layer of finite elements near the contact surface, imitating the sliding. At the axis of rotation OB ($r=0$) one has $\tau_{rz}=0$. Due to symmetry of the problem with respect to horizontal plane BC passing through the sample center, only the upper part of the sample is considered. At the plane of symmetry, $\tau_{rz}=0$, and the twisting displacements are $u_\varphi=0$. Then, one applies the half of the rotation angle $\varphi/2$ to the anvil. A quarter of a cross section of an axisymmetric sample after deformation is shown in Fig. 1. The initial thickness of the preindented part of a sample between flat diamond surfaces h_0 is one-tenth of an anvil diameter, $d_0=2R$, and one-half of the thickness of the nonindented part of the sample, the diameter of the disk was 3 d_0. The FEM code ABAQUS is implemented.[9] The loading path consists of two parts: first, material was compressed by the force Q, and then torsion was applied under fixed load. After each loading step the ABAQUS built-in remeshing procedure was performed.

In (Fig. 1), distributions of the σ_{rr} and σ_{zz} components of stress tensor have been presented for averaged normal stress $Q/S=F=5.89$ GPa (where S is the initial contact area equal to 2547 mm^2) and $\varphi=2.5$. Below the flat surface, σ_{zz} is practically independent of the z coordinate, while σ_{rr} decreases from the contact surface to the plane of symmetry. Both stresses grow linearly with decreasing r. Under the flat surface, $\tau_{r\varphi}$ is constant, and τ_{zr} is practically independent of r, except in the region near the symmetry axis.

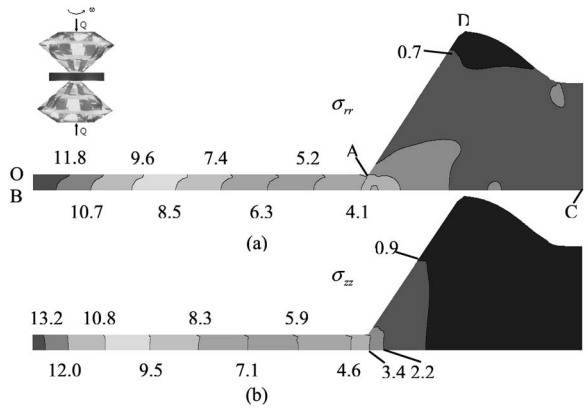

FIG. 1. Distribution of normal components σ_{rr} (a) and σ_{zz} (b) of the stress tensor for the averaged applied axial stress $F=5.89$ GPa and rotation angle $\varphi=2.50$ in a quarter of a cross section of the sample. BC is a plane of symmetry, OB is the axis of rotation, and OAD is the contact surface with an anvil. The inset shows the schematics of rotational diamond anvil cell.

[a]Electronic mial: valery.levitas@ttu.edu

 © 2007 American Institute of Physics
Downloaded 05 Oct 2007 to 129.118.17.179. Redistribution subject to AIP license or copyright, see http://apl.aip.org/apl/copyright.jsp

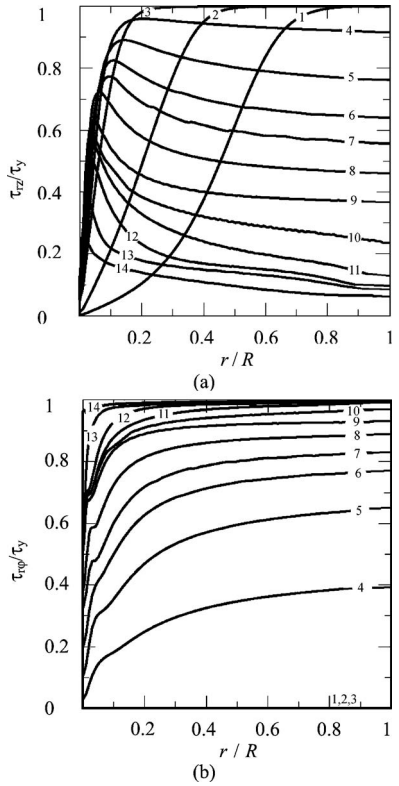

FIG. 2. Distribution of shear components τ_{rz} (a) and $\tau_{r\varphi}$ (b) of the stress tensor along the radius of the contact surface OA of a sample r for applied averaged axial stress $F=6.87$ GPa and various loading stages. For $\varphi=0$, F are 5.89 GPa (1), 6.65 GPa (2), and 6.87 GPa (3). For $F=6.87$ GPa, φ are 0.03 (4), 0.15 (5), 0.37 (6), 0.57 (7), 0.998 (8), 1.45 (9), 1.8326 (10), 1.8335 (11), 1.8362 (12), 1.852 (13), and 2.032 (14).

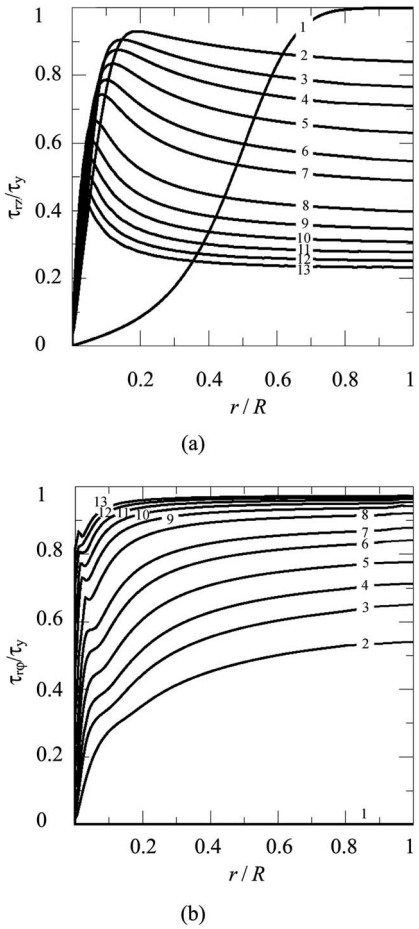

FIG. 3. Distribution of shear components τ_{rz} (a) and $\tau_{r\varphi}$ (b) of the stress tensor along the radius of the contact surface OA of a sample r for applied averaged axial stress $F=5.89$ GPa and various loading stages. For $F=5.89$ GPa φ are 0 (1), 0.03 (2), 0.09 (3), 0.15 (4), 0.27 (5), 0.478 (6), 0.6313 (7), 0.8455 (8), 1.0535 (9), 1.4535 (10), 1.6881 (11), 2.016 (12), and 2.368 (13).

Two problems with different initial compressions were solved. In the first case, compressive stress $F=6.87$ GPa was applied in such a way that τ_{rz} along OA reached its maximum value τ_y almost everywhere (Fig. 2). In the second case, $F=5.89$ GPa and τ_{rz} reached its maximum value along the external half of the radius only (Fig. 3). As torsion is applied, τ_{rz} in the region where it reached τ_y decreases with the growth of twisting shear stress $\tau_{r\varphi}$ because the total contact shear stress $\sqrt{\tau_{r\varphi}^2+\tau_{zr}^2}=\tau_y$. In the central part of the sample, τ_{rz} initially grows with rotation (Fig. 3), and corresponding distributions of normal axial stress σ_{zz} are shown in Fig. 4. If rotation starts when $\tau_{rz}=\tau_y$ in the major part of the contact surface, then pressure changes slightly during rotation of an anvil and in the central part of the sample only [Fig. 4(a)]. When rotation starts before τ_{rz} reaches τ_y in a significant portion of the sample, then τ_{rz}, the pressure gradient, and pressure grow in the central part during rotation of an anvil under constant force. This result suggests an additional reason for the pressure self-multiplication effect (i.e., for the increase in pressure under constant force) that was previously observed and explained during PT to a stronger phase only.[1,4,5]

During rotation of an anvil under constant axial force, the thickness of the sample decreases significantly (Fig. 5), an effect that is related to the reduction in τ_{rz} due to an increase in $\tau_{r\varphi}$ and that was predicted by the analytical solution.[4,5] In the case of PT, which is accompanied by the volume decrease, reduction in thickness compensates the volume decrease and increases pressure in the transforming region.[4,5] Thus, reduction in sample thickness represents the main macroscopic mechanism for promoting PT by the rotation of an anvil.

Distributions of the Odqvist parameter q (accumulated plastic strain)[8] along the height z for six sections with different r values are shown in Fig. 6 after compression (a) and torsion (b) by $\varphi=2.04$. Note that for homogeneous uniaxial compression $q=\ln(h_0/h)$, where h is the final thickness of the sample. However, contact shear strains increase q drastically. Thus, in Fig. 6(a), $\ln(h_0/h)=0.874$, which corresponds to q value in the vicinity of the plain of symmetry where plastic shears are absent. However, near the contact surface concentrated plastic shear increases from q to 1 and higher.

Rotation of an anvil increases q due to a decrease in sample thickness and especially due to localized plastic shear near the contact surface. The maximum value of q reaches 50. Enormous heterogeneity in plastic strain, in both the axial and radial directions, causes a significant problem in determination and interpretation of the kinetic data on strain-induced phase transformations (PTs) and chemical reactions. The volume fraction of a product phase can be currently measured locally.[3,10] When Raman spectra are used, volume fraction is averaged over the thin layer near the contact surface, in which plastic strain is much larger than in bulk. When x-ray diffraction is used, volume fraction is averaged over the thickness of a sample in the vicinity of a chosen point r. Thus, results have to be different, which was ob-

Downloaded 05 Oct 2007 to 129.118.17.179. Redistribution subject to AIP license or copyright, see http://apl.aip.org/apl/copyright.jsp

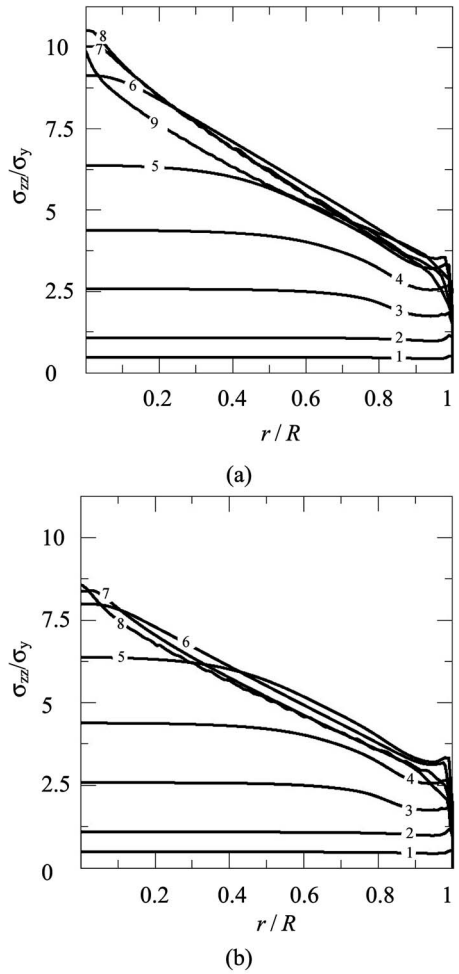

FIG. 4. Distribution of contact normal stress σ_{zz} along the radius of a sample r for applied averaged axial stresses F=6.87 GPa (a) and F=5.89 GPa (b) and various loading stages. For φ=0, F are 0.673 GPa (1), 1.523 GPa (2), 3.051 GPa (3), 4.58 GPa (4), 5.89 GPa (5), and 6.87 GPa (6). For F=6.87 GPa, φ are 0.67 (7), 1.45 (8), and 2.032 (9), (a). For φ=0, F are 0.673 GPa (1), 1.523 GPa (2), 3.051 GPa (3), 4.58 GPa (4), and 5.89 GPa (5). For F=5.89 GPa, φ are 0.03 (6), 0.646 (7), and 2.192 (8) (b).

served experimentally.[10] Significantly larger plastic strain along the contact surface than in the bulk suggests that strain-induced PTs and new strain-induced phases can be more easily detected in the contact layer.

In summary, the FEM solution for components of stress tensors and for accumulated plastic strain for the sample compressed and twisted in RDAC is found. The solution revealed the pressure self-multiplication effect during rotation of an anvil without phase transformation (for case 2) and significant heterogeneity of accumulated plastic strain, which has to be taken into account in determination of the kinetics of strain-induced PTs and chemical reactions.

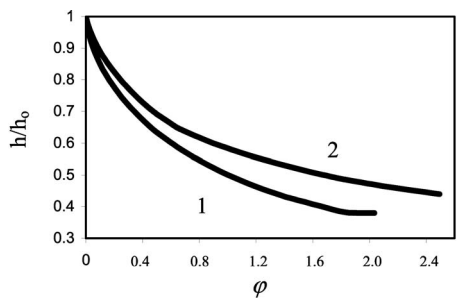

FIG. 5. Reduction of relative thickness of a sample vs rotation angle of an anvil under constant averaged axial stresses F=6.87 GPa (1) and F=5.89 GPa (2).

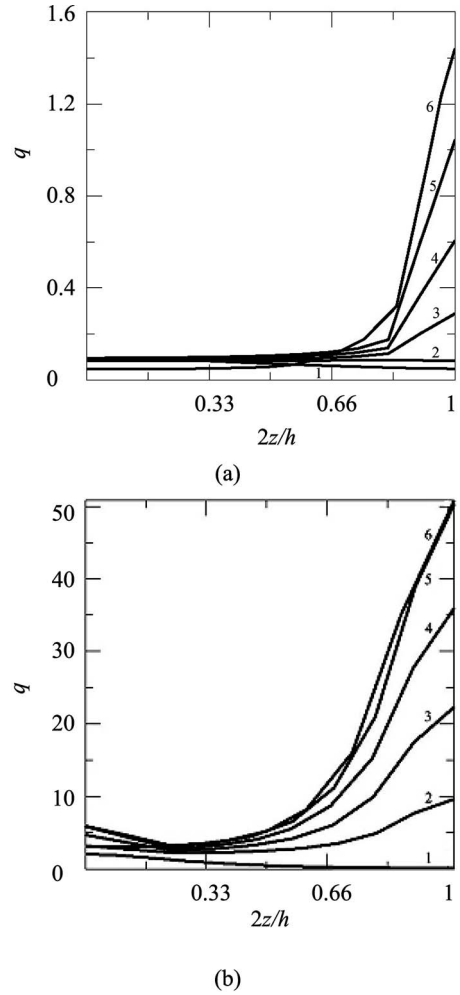

FIG. 6. Distributions of the Odqvist parameter q (accumulated plastic strain) along the height z for six sections with different r values after compression (a) and torsion by φ=2.04 (b): r/R=0 (1), r/R=0.2 (2), r/R=0.4 (3), r/R=0.6 (4), r/R=0.8 (5), and r/R=1 (6).

Support of NSF (CMS) is gratefully acknowledged.

[1]V. D. Blank, Yu. Ya. Boguslavski, M. I. Eremetz, E. S. Izkevich, Yu. S. Konyaev, A. M. Shirokov, and E. I. Estrin, Sov. Phys. JETP **87**, 922 (1984); M. M. Aleksandrova, V. D. Blank, A. E. Golobokov, Yu. S. Konyaev, and E. I. Estrin, Solid State Phys. **29**, 2573 (1987); M. M. Alexandrova, V. D. Blank, and S. G. Buga, *ibid.* **35**, 1308 (1993).
[2]N. V. Novikov, S. Polotnyak, L. Shvedov, and V. I. Levitas, J. Superhard Mater. **3**, 39 (1999).
[3]V. I. Levitas, Y. Ma, J. Hashemi, M. Holtz, and N. Guven, J. Chem. Phys. **25**, 044507 (2006).
[4]V. I. Levitas, Phys. Rev. B **70**, 184118 (2004).
[5]V. I. Levitas, in *High Pressure Surface Science and Engineering*, edited by Y. Gogotsi and V. Domnich (Institute of Physics, Bristol, 2004), p. 159.
[6]W. Moss and K. A. Goettel, Appl. Phys. Lett. **50**, 25 (1987); W. C. Moss, J. O. Hallquist, R. Reichlin, K. A. Goettel, and S. Martin, *ibid.* **48**, 125 (1986); S. T. Weir, J. Akella, C. Ruddle, T. Goodwin, and L. Hsiung, Phys. Rev. B **58**, 11258 (1998); S. Merkel, R. J. Hemley, and H. K. Mao, Appl. Phys. Lett. **74**, 656 (1999).
[7]V. I. Levitas, S. B. Polotnyak, and A. V. Idesman, Strength Mater. **3**, 221 (1996); N. V. Novikov, V. I. Levitas, and A. V. Idesman, High Press. Res. **5**, 868 (1990).
[8]V. I. Levitas, *Large Deformation of Materials with Complex Rheological Properties at Normal and High Pressure* (Nova Science, New York, 1996).
[9]ABAQUS, Hibbit, Karlsson and Sorensen, Inc., Ver. 6.2, 2001.
[10]V. Domnich, D. Ge, and Y. Gogotsi., in *High Pressure Surface Science and Engineering*, edited by Y. Gogotsi and V. Domnich (Institute of Physics, Bristol, 2004), Chap. 5.1, p. 381.

Downloaded 05 Oct 2007 to 129.118.17.179. Redistribution subject to AIP license or copyright, see http://apl.aip.org/apl/copyright.jsp